Catalysis Today 148 (2009) 103–108

Contents lists available at ScienceDirect

Catalysis Today

journal homepage: www.elsevier.com/locate/cattod

Photophysical and photocatalytic properties of nanosized copper-doped titania sol–gel catalysts

Rosendo López [a], Ricardo Gómez [a,*], María Elena Llanos [b]

[a] Universidad Autónoma Metropolitana-Iztapalapa, Departamento de Química, ECOCATAL, Av. San Rafael Atlixco No. 186, C.P. 09340 México D.F., Mexico
[b] Laboratorio de Caracterización de Materiales, Dirección de Investigación y Posgrado, Instituto Mexicano del Petróleo, Eje Central Lázaro Cárdenas No. 152, 07730 México D.F., Mexico

ARTICLE INFO

Article history:
Available online 2 May 2009

Keywords:
Sol–gel
Doped photocatalysts
Copper oxidation state
Band-gap energy
2,4-Dichlorophenoxyacetic acid degradation

ABSTRACT

The effect of doping the TiO_2 lattice with copper was studied. TiO_2–Cu semiconductors (0.1, 0.5, 1.0 and 5.0 Cu wt.%) were synthesized by the sol–gel method by incorporating Cu $(NO_3)_2$ into the titanium alkoxide solution. In the samples thermally treated at 500 °C, mesoporous materials (9.5–12 nm) with specific surface areas of 90–52 m^2/g were obtained. The X-ray diffraction (XRD) patterns of the annealed samples present anatase as the sole nanocrystalline phase (~28 nm). The UV–vis diffuse reflectance spectra of the Cu-doped samples show a shift in the band gap to lower energy levels. The X-ray photoelectron spectroscopy (XPS) reveals a reduction in the oxidation state of the copper precursor, Cu(II), stabilizing Cu(0) and Cu(I) in the annealed solids. The photocatalytic test for the 2,4-dichlorophenoxyacetic acid degradation showed high efficiency and mineralization up to 92% (total organic carbon, TOC) in the Cu-doped sol–gel materials. The enhancement of the photocatalytic activity was discussed as an effect due to the Cu content as well as to the formation of stable Cu(I) in the Cu-doped TiO_2 semiconductors.

© 2009 Elsevier B.V. All rights reserved.

1. Introduction

Among the semiconductor oxides, titania has been widely used as the most suitable material for environmental photocatalytic applications. However, the preparation of improved titania-based photocatalytic materials has continuously been the goal of many laboratories around the world. To improve the photocatalytic properties of TiO_2, various metals and oxides have been used as doping agents in order to prepare photocatalysts with improved properties for the degradation of organic pollutants. The cationic doping of TiO_2 has been successfully obtained by the incipient impregnation of the semiconductor with metallic cations [1,2]; however, because of the aforesaid preparation method, the doping effect has been limited to the solid surface and titania structural modifications, which allow to improve its photophysical properties are not attained. In this way, the sol–gel preparation has been found to be an effective method for the TiO_2 lattice ion incorporation. For the instance, the incorporation of copper nitrate during the gelling step allows the cationic substitution of Ti^{4+} by Cu^{2+} in the titania network [3–6]. The doping with metal ions induces effects on the photocatalytic activity of TiO_2. Some authors claim that the metal doping should decrease the photothreshold energy of TiO_2, producing a significant band gap narrowing, which allows to lower the energy consumption; meanwhile, other authors consider that the metal doping could work as a recombination center for electrons and holes, avoiding a fast recombination; and thus increasing the TiO_2 photoreactivity [7–9]. In the present work, copper-doped titania photocatalysts with different copper contents (0.1, 0.5, 1.0 and 5.0 wt.%) were prepared by the sol–gel method in order to increase the copper effects on TiO_2. The doped semiconductors were prepared with various Cu contents, and their characterization was performed by means of nitrogen adsorption, X-ray diffraction (XRD), UV–vis spectroscopy and X-ray photoelectron spectroscopy (XPS). The photocatalytic activity was evaluated for the 2,4-dichlorophenoxyacetic acid degradation, which is an important pollutant herbicide. In this work, copper was chosen as doping agent because it has been reported previously that copper is a good doping element that improves the TiO_2 photocatalytic performance [10–13].

2. Experimental procedure

2.1. Preparation of photocatalysts

The TiO_2–Cu (metal load: 0.1, 0.5, 1.0, 5.0 wt.%) solids were prepared by the sol–gel method as follows: the corresponding amount of hydrated copper(II) nitrate (Aldrich 99.99%) to obtain

* Corresponding author. Tel.: +52 55 58044668; fax: +52 55 58044666.
E-mail addresses: ross@xanum.uam.mx (R. López), gomr@xanum.uam.mx (R. Gómez).

0920-5861/$ – see front matter © 2009 Elsevier B.V. All rights reserved.
doi:10.1016/j.cattod.2009.04.001

the stated Cu contents was added to a flask containing 18 mL of deionized distilled water, 44 mL of 1-butanol (Aldrich 99.4%) and 0.2 mL of nitric acid (Aldrich 70% in water to obtain pH 3). Afterwards, 44 mL of titanium(IV) butoxide (Aldrich 97%) were added dropwise to the solution during 4 h (water/alkoxide molar ratio of 8). The gelling solution was then heated at 70 °C under reflux and maintained with constant stirring for 24 h at 70 °C until the gel was formed. The resulting xerogels were dried at 70 °C for 24 h. The dried solids were ground in an agate mortar until a fine and homogeneous powder mixture was obtained. Finally, the samples were calcined in air at 500 °C for 4 h using a heating rate of 2 °C/min. A reference TiO_2 sol–gel sample was prepared according to the protocol described above for the TiO_2–Cu samples.

2.2. Characterization

The XRD was used to examine the crystalline phases of the samples. The specimens were prepared by packing the powder samples in a glass holder. The X-ray diffraction patterns were collected at room temperature with a Siemens D-500 diffractometer operated at 40 kV and 30 mA. The Cu Kα radiation was selected using a graphite monochromator. The measurements were recorded in steps of 0.03° with a count time of 1 s in the 2θ range of 5–70°:

$$D = \frac{K\lambda}{B\cos\Theta}$$

The crystallite size was estimated using Scherrer's formula, where B is the full width at half maximum (FWHM) of the XRD peak, K is a constant ($K = 0.94$), Θ is the diffraction angle and λ is the X-ray wavelength corresponding to Cu Kα radiation (λ = 1.5405 Å).

The UV–vis diffuse reflectance spectroscopy (UV–vis DRS) was used to estimate the band gap of the samples. Self-supporting pellets were prepared and the spectra were obtained with a Varian Cary 100 UV–vis spectrophotometer equipped with an integrating sphere for diffuse reflectance studies. Magnesium oxide (MgO) was used as a reference (100% reflectance standard). The diffuse reflectance spectrum was obtained and transformed to a magnitude proportional to the extinction coefficient (α) through the Kubelka–Munk function:

$$F(R) = \frac{(1-R)^2}{2R}$$

The E_g was then calculated from the plot of the modified Kubelka–Munk function, $[F(R) \times h\nu]^{1/2}$ vs energy of the absorbed light.

The XPS was used to analyze the oxidation state of the metal doping in the titania semiconductors. A Thermo VG Scientific ESCALAB 250 electron spectrometer equipped with hemispherical analyzer equipment was used in these studies. The spectrometer was operating at constant pass energy mode, and monochromatized Al Kα radiation ($h\nu$ = 1486.6 eV) was used. The X-ray source operated at 10 mA and 15 kV. The intensities of the peaks were estimated by calculating the integral of each peak after subtracting the S-shaped background and fitting the experimental peak to a combination of Lorentzian/Gaussian lines of variable proportions. The binding energies (BE) were referenced to the C (1s) peak, which was fixed at 284.6 eV.

The specific surface areas of the catalysts were determined by the BET method from the nitrogen adsorption isotherms obtained with a Quantachrome Autosorb-3B apparatus; this equipment has the flexibility to apply multiple methods of analyses at the same time, as multipoint BET and BHJ pore size distribution from the desorption isotherms. Before adsorption, the samples were desorbed in vacuum at 300 °C for 10 h. The mean pore size diameter distribution was calculated from the desorption branch of the isotherm by applying the BJH method.

2.3. Photocatalytic evaluation

The photocatalytic activity of the samples was evaluated for the 2,4-diclorophenoxyacetic acid degradation. The evaluation was carried out in a glass reactor containing the aqueous solution with 30 ppm of the herbicide and 0.2 g of catalyst. The powder suspension was stirred and irradiated with a high pressure mercury lamp (emitting radiation of 254 nm, 2.16 W, 18 mA) protected with a quartz tube and immersed in the solution. To assure the adsorption–desorption equilibrium of the molecule in the solution, the suspension was stirred for 30 min in the dark with an air flow of 1 mL/s (Air-Pump BOYU S-4000B), and then irradiated with the UV lamp (Pen-Ray UVP). The degradation of the pollutant was monitored by following the main section of the 2,4-D absorption band at 284 nm using a UV–vis spectrophotometer Varian Cary 100 UV–vis. In addition, total organic carbon (TOC) measurements were carried out with a TOC-VCSN Shimadzu (NDIR detector) in order to know whether the 2,4-D mineralization was achieved.

3. Results and discussion

3.1. Structural analysis

3.1.1. X-ray diffraction (XRD)

The X-ray diffraction patterns of the copper-doped titania samples annealed at 500 °C are shown in Fig. 1. In all the samples, the peaks corresponding to the formation of the anatase phase can be observed, showing that the incorporation of Cu preserves the anatase structure at temperatures around 500 °C. It must be noted that the presence of copper oxide cannot be observed even in the sample with the highest copper content. In the amplification of the anatase peak (1 0 1), a notable shift in the copper-doped samples in comparison with the reference TiO_2 JCPDS 21-1272 (Fig. 2) can be seen. The displacement of the (1 0 1) reflection can be due to some perturbation in the anatase crystalline phase. The similarity in the Cu and Ti ionic radii (0.72 Å for Cu and 0.68 Å for Ti) allows the interstitial incorporation of the dopant into the titania network. Cu could be placed in the interstitial sites due to $r_{Ti} < r_{Cu}$ producing the strain of the titania lattice, and hence a displacement of the (1 0 1) signal in the XRD pattern. On the other hand, the crystallite size calculated by Scherrer's formula is listed in Table 1, where it

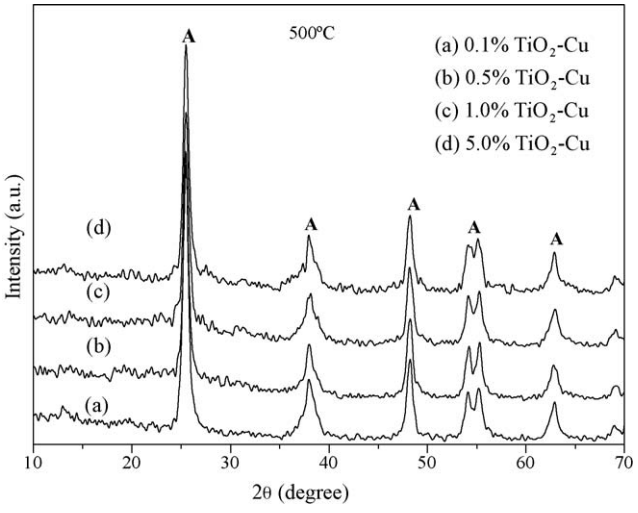

Fig. 1. (a–d) X-ray diffraction patterns of the TiO_2–Cu materials annealed at 500 °C.

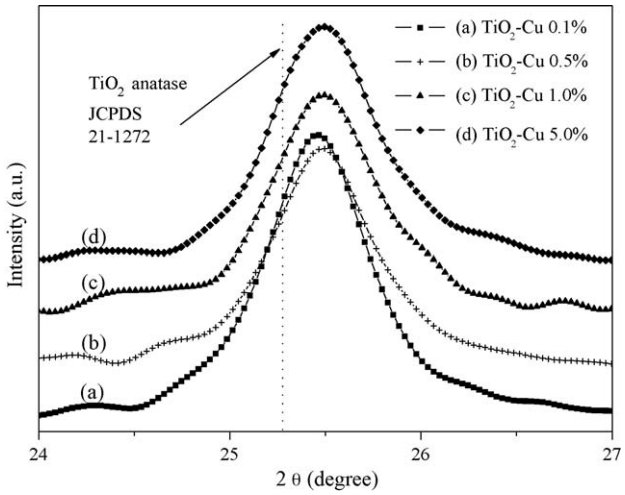

Fig. 2. (a–d) XRD peak for the (1 0 1) reflection for the Cu-doped TiO_2 samples.

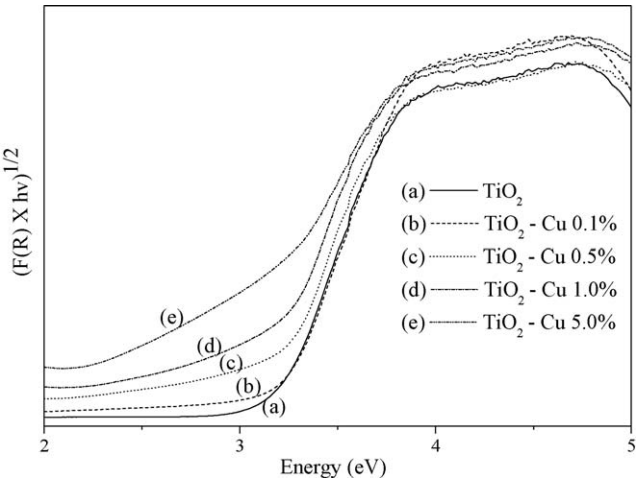

Fig. 4. (a–e) Kubelka–Munk modified spectra for the TiO_2–Cu semiconductors.

Table 1
Average crystallite size and E_g values for the Cu doping samples.

TiO_2–Cu (wt.%)	Crystallite size (nm)	E_g (eV)
TiO_2	40.5	3.28
0.1	30.4	3.19
0.5	29.3	3.13
1.0	26.7	3.05
5.0	29.0	2.81

can be seen that the solids are nanostructured with crystallite sizes comprised between 30.4 and 26.7 nm.

3.1.2. UV–vis diffuse reflectance spectroscopy (UV–vis DRS)

The UV–vis DRS spectra for the different TiO_2–Cu materials are shown in Fig. 3, where the effect of the copper content on the absorption spectra is clearly evidenced. In Fig. 3(a) and (b), the absorption bands of TiO_2 and TiO_2–Cu (0.1 wt.%) at around 400–316 nm can be observed, additionally to a large absorption band (400–800 nm) due to the $O^{2-}(2p) \rightarrow Ti^{4+}$ (3d) transitions in the tetrahedral symmetry [14,15]. In the samples with low copper doping, the TiO_2 absorption spectrum was not substantially modified. However, in the samples with 0.5, 1.0 and 5.0 Cu wt.% (Fig. 3(c)–(e), respectively), besides a strong absorption band between 550 and 316 nm, a broad absorption band at 800–500 nm can be observed. This absorption band can be assigned to the Cu^{2+} and Cu^{1+} oxidation states. The bands between 800 and 500 nm are assigned to the $2E_g \rightarrow 2T_{2g}$ transitions of Cu^{2+} as well as to the presence of Cu^{1+} clusters reduced from the Cu–O matrix [16]. In Fig. 4, the reflectance measurements obtained with the Kubelka–Munk function given by $F(R) = (1 - R)^2/2R$ are presented, where R is the sample reflectance [17,18]. $F(R)$ indicates the absorptivity of the sample at a particular wavelength, which is proportional to the absorption constant of the material. The absorption edge energy (E_g) was obtained through the plot of the modified Kubelka–Munk (Table 1), where a shift in the visible region from 3.28 to 2.81 eV for the TiO_2 and TiO_2–Cu 5 wt.% semiconductors can respectively be seen. These results suggest that at low doping copper content (0.1, 0.5 and 1.0 Cu wt.%), the narrowing of the band gap could be due to the cationic substitution of titanium by copper. On the other hand, at a high doping content (5.0 Cu wt.%), the cationic substitution and the formation of copper oxide clusters on the titania surface that play the role of electron traps could produce a diminution of the fast electron–hole recombination together with a band gap narrowing effect.

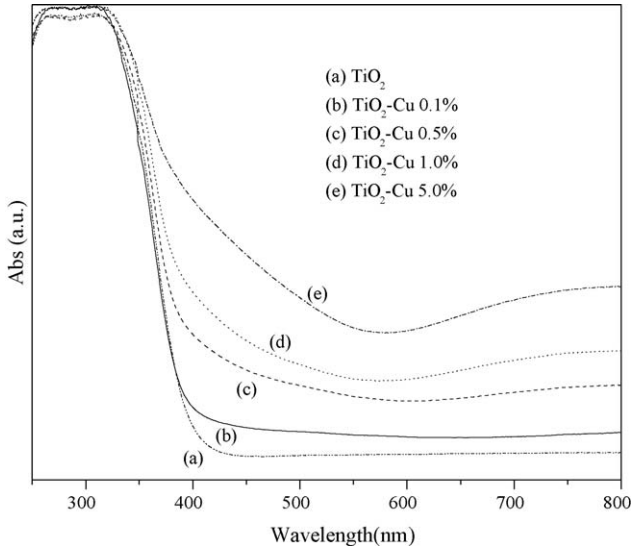

Fig. 3. (a–e) UV spectra for the Cu-doped TiO_2 semiconductors.

3.1.3. Nitrogen adsorption

The selected adsorption–desorption isotherms for the TiO_2–Cu samples annealed at 500 °C, are shown in Fig. 5. The isotherm shapes at all doping contents correspond to type IV, which is

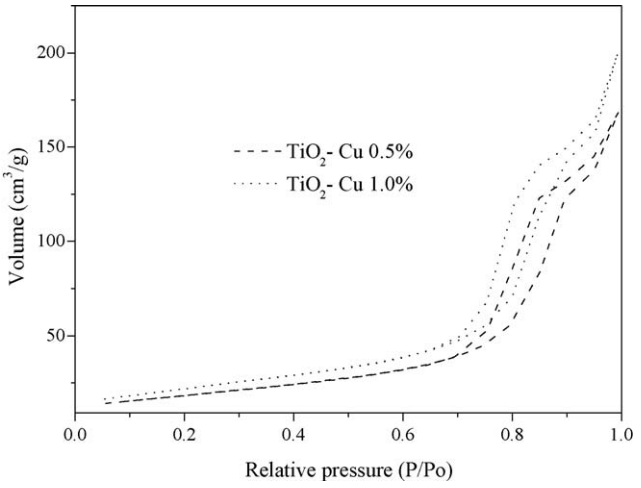

Fig. 5. Nitrogen adsorption isotherms for the selected TiO_2–Cu samples.

Table 2
Specific surface area, pore volume and mean pore size for the TiO_2–Cu photocatalysts.

Doping (wt.%)	Temp. (°C)	Specific surface area (m^2/g)	Pore volume (cm^3/g)	Pore size (nm)
0.1	500	89	0.33	9.5
0.5	500	76	0.31	12.1
1.0	500	80	0.30	12.3
5.0	500	52	0.22	12.1
TiO_2	500	70	0.27	12.1
P25	–	50	0.64	3.1

associated with capillary condensation taking place in the mesoporous solids (2–50 nm), and present an H1-type hysteresis loop according to IUPAC classification [19]. The calculated BET specific surface area, mesopore volume and pore size diameter for all the samples are listed in Table 2. The results show that minor copper effects on the specific surface areas as well as on the mesopore volume or pore size diameter can be observed in the semiconductors with low copper contents, whereas the sample with 5.0 Cu wt.% (52 m^2/g) shows a notable specific surface area diminution of around 45% in comparison with the solid with a Cu content of 0.1 wt.% (89 m^2/g). The BET specific surface areas are of the same order in all doped and undoped samples with the exception of the TiO_2–Cu 5 wt.% sample that shows the lowest BET specific surface area. Thus, the presence of copper nitrate in the gelling solution does not modify the hydrolysis-condensation titanium alkoxide reactions, and the lowest BET specific surface area showed by the TiO_2–Cu 5 wt.% sample could be due to the blockage of the pores by the copper oxide clusters formed over the titania surface.

3.1.4. X-ray photoelectron spectroscopy (XPS)

The XPS analysis was carried out to identify the oxidation state of copper in the nanostructured TiO_2–Cu samples. The survey and amplification of the selected spectra are respectively shown in Figs. 6 and 7. In Fig. 6, the characteristic peaks for the C 1s, Ti 2p, O 1s and Ti 2s core level binding energy (BE) in the 200–600 eV region can be seen. The C 1s peak (284.5 eV) corresponds to carbon, which is always present on the surface of the powdered samples (adventitious carbon). On the other hand, in the 960–920 eV binding energy region, the peak for the Cu 2p core level (BE) can be seen, whose intensity increases with the Cu content (samples with 0.5, 1.0 and 5.0 Cu wt.%). Unfortunately, for the samples with 0.1 Cu wt.%, the XPS equipment does not detect the Cu 2p spectrum, which is most probably due to the low content of copper in the sample. In Fig. 7, the deconvolution of the Cu 2p signal for the selected samples was resolved in Cu $2p_{1/2}$ and Cu $2p_{3/2}$ core level peaks, identifying the Cu^0 and Cu^{1+} copper species. The presence of copper in the Cu^{2+} oxidation state can be excluded because of the absence of the characteristic shake-up satellite lines of CuO, which are attributed to shake-up transitions by a ligand-metal 3d charge transfer that does not occur with Cu^0 and Cu^{+1} species, which have completely filled 3d shells [20]. In the deconvoluted spectra, a shift in the Cu^{1+} $2p_{3/2}$ peak to a higher energy level is observed and the corresponding BE for the different samples are listed in Table 3. This shift became more important in the sample with the highest copper content; however, the energy difference between the Cu $2p_{3/2}$ and the Cu $2p_{1/2}$ peaks of 20.0 eV was maintained constant at any copper content. A qualitative evaluation of the Cu^{1+} content and the Cu^0 species in the sample was done by using the full width at half maximum (FWHM) value of the Cu 2p spectrum [21,22]. When the doping percentage increases, a low Cu^{1+}/Cu^0 ratio is obtained. Such an important formation of Cu^0 was obtained at high copper contents (Table 3). The copper in the precursor has an oxidation state of Cu(II), however, in the sol–gel samples, it was reduced to either Cu(I) or Cu(0). This metallic reduction effect was attributed to the dehydroxilation step, where OH radicals with strong reducing proprieties were produced [23]. The effect was observed in Pt/

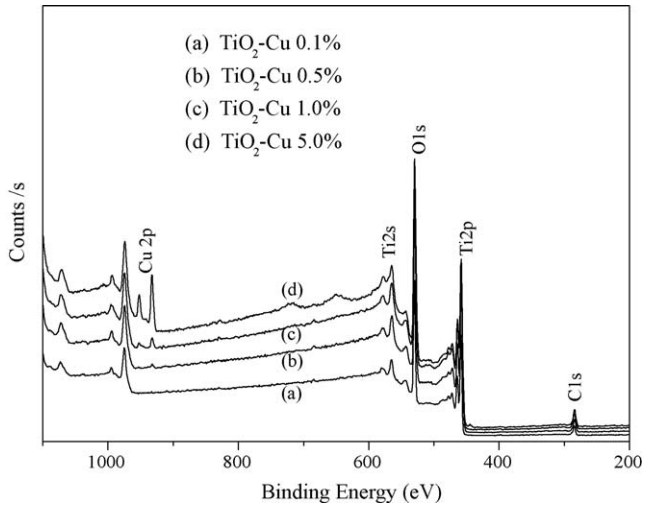

Fig. 6. (a–d) X-ray photoelectron spectra (survey) for the TiO_2–Cu semiconductors.

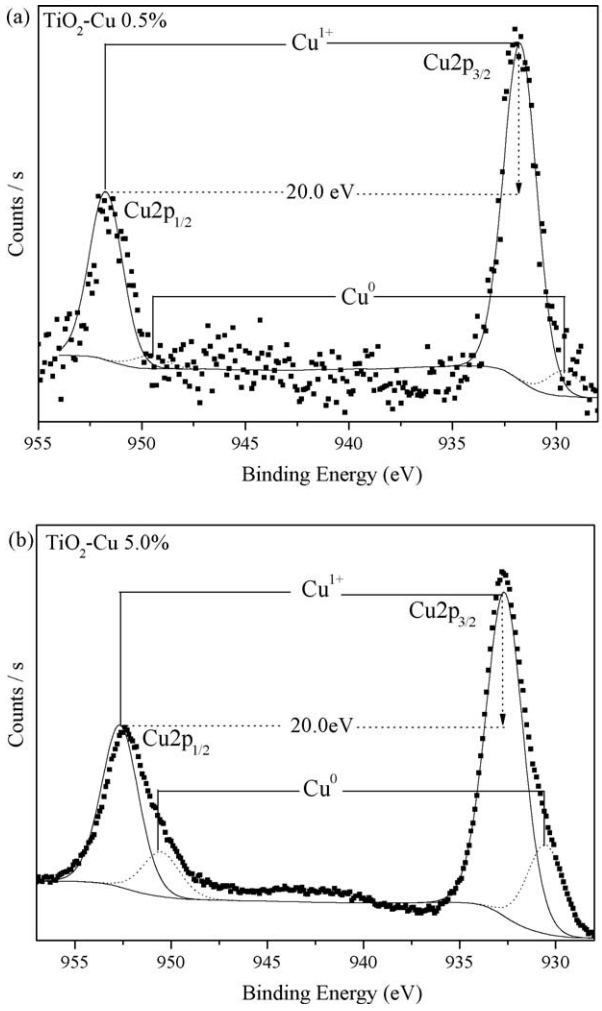

Fig. 7. X-ray photoelectron spectra, deconvolution of the Cu 2p peak: (a) 0.5 wt.% and (b) 5.0 wt.%.

Table 3
XPS analysis for the TiO_2–Cu samples.

Sample (wt.%)	Binding energy (eV)				FWHM	Cu^0/Cu^{1+} (%)
	Cu $2p_{3/2}$ Cu^{+1}	Cu $2p_{1/2}$ Cu^{+1}	Cu $2p_{3/2}$ Cu^0	Cu $2p_{1/2}$ Cu^0	Cu $2p_{3/2}$ Cu^{+1}	
0.5	931.74	951.74	929.64	949.64	1.96	7/93
1.0	932.18	952.18	930.07	950.07	2.01	12/88
5.0	932.66	952.66	930.52	950.52	2.37	22/78

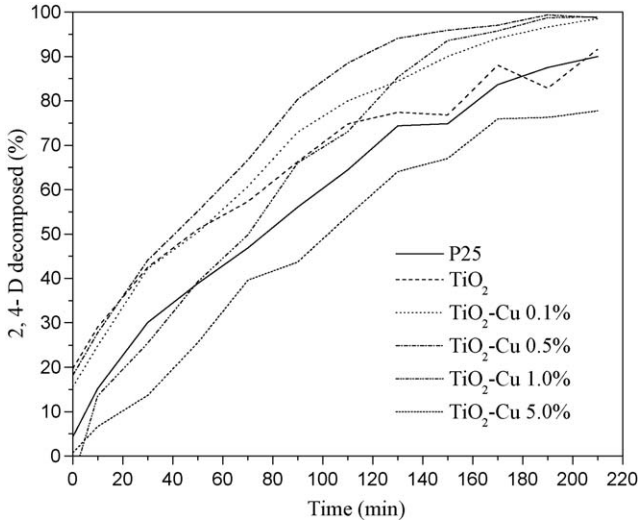

Fig. 8. Photocatalytic activity for the 2,4-D decomposition as a function of time.

MgO, where the formation of Pt^0 after annealing the sol–gel samples was obtained without reducing agent [24]. It is interesting to mention that no signal of nitrogen (from precursor) was observed in our preparations since the XPS signal should be at 397.2 eV, which is assigned to the N 1s spectrum.

3.1.5. Photocatalysis

After mixing the TiO_2–Cu samples in the 2,4-D solution for 30 min in the dark, the photocatalytic degradation of the herbicide was followed over a period of 2 h, and the photocatalytic activity as a function of time for the various samples is shown in Fig. 8. Fig. 9 shows that the photocatalytic degradation corresponds to a pseudo-first-order reaction. Pseudo-first-order kinetics was assumed to calculate the corresponding degradation rate constant (k):

$$\ln\left[\frac{C}{C_0}\right] = -kt$$

where C_0 is the initial concentration in (mg/L), C is the concentration (mg/L) at a given time t (s or min) and k is the first-order degradation rate constant (min^{-1} or s^{-1}). Half-life, $t_{1/2}$ (min or s), can be calculated from k by using the following equation:

$$t_{1/2} = \frac{\ln 2}{k}$$

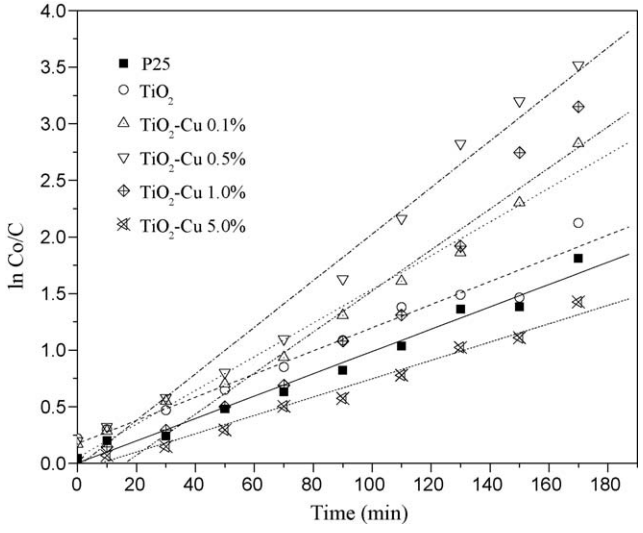

Fig. 9. First-order kinetics for the 2,4-D photodegradation on the Cu-doped TiO_2 semiconductors.

The photoactivity was calculated and reported as $t_{1/2}$ in Table 4. The results show that $t_{1/2}$ increases (44, 49, 71 and 89 min^{-1}) with the copper content in the catalysts (0.5, 0.1, 1.0 and 5.0 Cu wt.%), respectively. The highest activity of the samples with the lowest copper content can be the result of the Cu(I) amount in the samples since the Cu(I)/Cu(0) ratio is higher for the samples with low copper contents. The role of Cu(I) in the photoactivity could be related to the capacity of Cu(I) as electron captor inducing a low electron–hole recombination. As a result, the photoactivity was enhanced in the samples with the lowest Cu(I) content. From the prepared catalysts, only one of them (5.0 Cu wt.%) showed a band gap in the visible region (2.81 eV). However, the photoactivity with visible light source was performed on TiO_2 and TiO_2–Cu 5 wt.% samples. The study showed no activity in both catalysts. This result suggests that the band gap value of 2.81 eV is the result of combined effects: cationic substitution and electron trap by the copper oxide clusters found on the titania surface. The shift in the visible region is then an artifact produced by the surface defects, and hence without important modifications of the TiO_2 band gap [25].

TOC determinations after 210 min of irradiation were made in all the samples. The mean amount of TOC for the initial solution before the photocatalytic probes was 19 mg/L. The TOC analyzed in the solution after 210 min of irradiation showed residual concentrations of organic carbon of 1.99 ppm for the samples with low Cu contents, and of 5.22 ppm for the 5.0 Cu wt.% sample (Table 4). These results show that high photoactivity and mineralization of the 2,4-D higher than 90% can be obtained with the TiO_2–Cu sol–gel samples in the present study. The role of the possible intermediates: 2,4-diclorophenol (2,4-DCP), chlorohydroquinone (CHQ) and 1,2,4-trichlorobenzene reported elsewhere

Table 4
Kinetic values for the 2,4-D photodecomposition and total organic carbon TOC for the TiO_2–Cu semiconductors.

Doping (wt.%)	k[a] (min^{-1})	$t_{1/2}$ (min)	TOC[b] (mg/L)	TOC[c] (%)
0.1	15.7	44	1.99	90
0.5	14.1	49	1.89	91
1.0	9.7	71	1.50	92
5.0	7.7	89	5.22	72
TiO_2	9.0	47	5.30	73
P25	8.8	77	4.94	74

[a] Rate constant.
[b] TOC 2,4-D residual.
[c] 2,4-D removed.

for the 2,4-D decomposition [26,27] is not considered in the present study because of the high mineralization obtained in the irradiated solutions after the photocatalytic test.

4. Conclusions

The preparation of Cu-doped titania by the sol–gel method allows the formation of nanocrystalline anatase with a crystallite size of around 30 nm. A shift in the 2θ of the (1 0 1) reflection for the anatase phase suggests an insertion of Cu species into the titania network. It was found that copper induces a shift in the energy band gap to lower energies, which change from 3.19 to 2.81 eV for the samples with low and high Cu contents, respectively. In the TiO_2–Cu samples, only slight effects on the textural properties were observed for the samples with low copper contents (76–89 m^2/g), whereas the sample with the highest copper content showed an important diminution in the BET area (52 m^2/g). The presence of Cu(0) and Cu(I), evidenced by XPS, confirms the reduction of Cu(II) during the dehydroxylation step occurring during the annealing of the samples. The stabilization of Cu(I) by TiO_2 seems to be the responsible of the high photoactivity and high 2,4-D mineralization shown by the samples with the highest Cu^{1+}/Cu^0 ratios.

Acknowledgements

R. López acknowledges the scholarship by CONACYT México. R. Gómez acknowledges the CONACYT CB-2006-1-62053 grant: "Preparation of semiconductors by the sol–gel method".

References

[1] M.I. Litter, Appl. Catal. B: Environ. 23 (1999) 89.
[2] J.M. Herrmann, Catal. Today 53 (1999) 115.
[3] G. Córdoba, M. Viniegra, J.L.G. Fierro, J. Padilla, R. Arroyo, J. Solid State Chem. 138 (1998) 1.
[4] X. Bokhimi, A. Morales, O. Novaro, T. López, O. Chimal, M. Asomoza, R. Gómez, Chem. Mater. 9 (1997) 2616.
[5] H. Kobayashi, N. Takezawa, M. Shimokawabe, K. Takahasi, In Preparation of Catalysts, vol. 3, Ed. Elsevier, Amsterdam, 1983, p. 696.
[6] F.S. Delk, A. Vavere, J. Catal. 85 (1984) 380.
[7] W.Y. Choi, A. Termin, M.R. Hoffmann, J. Phys. Chem. 98 (1994) 13669.
[8] S. Karvinen, P. Hirva, T.A. Pakkanen, J. Mol. Struct. THEOCHEM 626 (2003) 271.
[9] M. Maeda, T. Yamada, J. Phys.: Conf. Ser. 61 (2007) 755.
[10] K. Song, J. Zhou, J. Bao, Y. Feng, J. Am. Ceram. Soc. 91 (2008) 1369.
[11] L.Y. Zhao, P.C. Yang, X.K. Wang, Y.N. Xie, N.Z. Wu, Y.C. Xie, Appl. Surf. Sci. 228 (2004) 257.
[12] P.O. Larsson, A. Andersson, L.R. Wallenberg, B. Svensson, J. Catal. 163 (1996) 279.
[13] P.O. Larsson, A. Andersson, J. Catal. 179 (1998) 72.
[14] R. Sanjinés, H. Tang, H. Berger, F. Gozzo, G. Margaritondo, F. Lévy, J. Appl. Phys. 75 (1994) 2945.
[15] J. Chen, L.-B. Lin, F.-Q. Jing, J. Phys. Chem. Solids 62 (2001) 1257.
[16] G. Colón, M. Maicu, M.C. Hidalgo, J.A. Navío, Appl. Catal. B: Environ. 67 (2006) 41.
[17] P. Kubelka, F. Munk, Z. Tech. Phys. 12 (1931) 593.
[18] P. Kubelka, J. Opt. Soc. Am. 38 (1948) 448.
[19] IUPAC, Pure Appl. Chem. 57 (1985) 603.
[20] C.D. Wagner, W.M. Riggs, L.E. Davis, J.F. Moulder, G.E. Mullenberg, Handbook of X-ray Photoelectron Spectroscopy, Perkin-Elmer Corp.
[21] S.B. Kim, J.Y. Lee, H.T. Jang, J. Ind. Eng. Chem. 9 (2003) 440.
[22] B.F. Dzhurinskii, D. Gati, N.P. Sergushin, V.I. Nefedov, Russ. J. Inorg. Chem. 20 (1975) 2307.
[23] R. Gómez, T. López, X. Bokhimi, E. Muñoz, J.L. Boldú, O. Novaro, J. Sol–Gel Sci. Technol. 11 (1998) 309.
[24] X. Bokhimi, A. Aceves, O. Novaro, T. López, R. Gómez, J. Phys. Chem. 99 (1995) 14403.
[25] N. Serpone, J. Phys. Chem. B 110 (2006) 24287.
[26] M. Trillas, J. Peral, X. Domenech, Appl. Catal. B: Environ. 5 (1995) 377.
[27] O.M. Alfano, R.J. Brandi, A.E. Cassano, Chem. Eng. J. 82 (2001) 209.